ADVANCED OPTICAL MATERIALS
www.advopticalmat.de

Enhanced Renal Carcinoma Treatment via Synergistic Photothermal/Photodynamic Therapy Using Hittorf's Phosphorus-Decorated Polymeric Carbon Nitride Heterostructure

Chen Guan, Chenyu Li, Chengyu Yang, Dongjiang Yang, Lixue Zhang, Lingyu Xu, Ke Liu, Ningxin Zhang, Tianyang Li, Zhuo Song, Lin Che, Yanfei Wang, Liwei Zhang, Daohao Li, Yukun Zhu,* and Yan Xu**

Nanostructured heterojunctions offer a promising solution to overcome the limitations of narrow absorption spectra, limited penetration depths, and potential harm to healthy cells in phototherapy for clear cell renal cell carcinoma (ccRCC) treatment with nanomaterials. In this study, a heterostructure (PCN@HP) by decorating Hittorf's phosphorus nanorods onto biocompatible polymeric carbon nitride (PCN), enabling excitation by NIR light is designed. Compared with PCN and HP alone, the synthesized heterostructure generated localized heat upon broad absorption spectra of irradiation, boosting charge migration and separation, generating cytotoxic reactive oxygen species (ROS). Then, via in vitro and in vivo experiments, it is confirmed that the NIR-mediated PCN@HP heterojunction is a safe and effective approach for synchronous photothermal and photodynamic therapy treatment of ccRCC. Collectively, the PCN@HP heterojunction holds great potential as a non-invasive synergistic, dual-mode therapeutic nanomedicine for efficient tumor nano-therapy.

1. Introduction

Renal cell carcinoma represents a highly vascularized variant of kidney cancer, comprising almost 90% of all renal malignancies. Clear cell renal cell carcinoma (ccRCC), constituting around 75% cases, stands as the predominant yet aggressive pathological subtype.[1–3] Given the limited response of ccRCC to traditional interventions, various experimental treatments have been developed over time, including immune checkpoint blockade and combination regimens therapy.[4] However, the clinical application of these approved targeted agents is constrained due to inevitable toxicity and the emergence of drug resistance. Therefore, there is an urgent need for efficacious and safe therapies that specifically target ccRCC.[5–7]

Photothermal therapy (PTT) and photodynamic therapy (PDT) have been extensively utilized in cancer treatments, offering advantages such as low toxicity, minimal side effects, and reduced drug resistance.[8,9] Upon near-infrared (NIR) light irradiation, PTT involves the release of vibrational energy through photosensitizers, resulting in the generation of local heat.[10] This process, in turn, triggers hyperthermia-induced cell death. On the other hand, PDT entails a photochemical reaction that occurs when a photosensitizer, light, and oxygen interact. This interaction ultimately leads to the production of cytotoxic reactive oxygen species (ROS), which

C. Guan, C. Li, C. Yang, L. Xu, N. Zhang, T. Li, Z. Song, L. Che, Y. Wang, Y. Xu
Department of Nephrology
the Affiliated Hospital of Qingdao University
16 Jiangsu Road, Qingdao 266003, China
E-mail: xuyan@qdu.edu.cn

The ORCID identification number(s) for the author(s) of this article can be found under https://doi.org/10.1002/adom.202303318

DOI: 10.1002/adom.202303318

D. Yang, K. Liu, D. Li, Y. Zhu
State Key Laboratory of Bio-fibers and Eco-textiles
School of Environmental Science and Engineering
Qingdao University
308 Ningxia Road, Qingdao 266071, China
E-mail: lidaohao@qdu.edu.cn; yukunzhu@qdu.edu.cn

L. Zhang
College of Chemistry and Chemical Engineering
Collaborative Innovation Center for Hydrogen Energy Key Materials and Technologies of Shandong Province
Qingdao University
Qingdao 266071, China

L. Zhang
Institute of Diabetes and Regeneration Research
Helmholtz Diabetes Center
Helmholtz Center Munich
85764 Neuherberg, Germany

induces cell death.[11,12] However, the application of PTT may be limited by its side effects, such as hyperthermia-induced injury to healthy cells and tissues, while PDT can result in cytotoxic ROS that also cause damage to non-tumor cells.[13] To address these challenges, a contemporary approach has been proposed to synergistically combine PTT with PDT, thereby overcoming the individual limitations while still harnessing both therapies' benefits for tumor treatment.[14–16] The simplest approach to achieve synergistic performance in PDT and PTT involves the utilization of a single light absorber, followed by processing through the same light source and transmission system.[17] However, nanoparticle design often suffers from the complexity of formulations and multiple components, which hinder characterization and amplification processes, leading to irreproducible outcomes.[18] Although certain "one-for-all" materials like CuS, Ag_2S, and MoS_2 demonstrate potential for synergistic NIR-mediated PTT and PDT, their long-term usage in the human body is unsuitable due to bioaccumulation tendencies and resistance to degradation.[19–21] Therefore, there remains a significant gap in finding a viable nanoplatform that exhibits synergistic PTT/PDT performance while enabling effective tumor ablation.

Heterojunction refers to the interface region formed by coupling two different functional materials.[22] It encompasses various compounds, possesses numerous unique functions, and retains the properties of each individual component. This combination provides a novel "one-for-all" strategy for integrating PTT and PDT treatments for deep-seated tumors.[22,23] Recently, metal-free polymeric carbon nitride (PCN) based heterojunctions composed primarily of two earth-abundant elements (e.g., carbon and nitrogen) have garnered significant interest in diverse biomedical applications due to their distinctive physicochemical properties, versatile surface functionalization capabilities, ultrahigh surface area, and excellent biocompatibility.[24,25] However, its light absorption edge below 460 nm limits its practical applications in the NIR range.[26] Phosphorus (P) doping is a typical method for effectively improving the performance of PCN. It remarkably changes the electronic structure and extends the light absorption to cover almost the full-range spectra.[27–30] Red phosphorus (RP), as a bio-photocatalyst for PTT with a broad solar light absorption up to 700 nm,[14,31–33] is a potential candidate for the PCN heterostructure to facilitate interaction with longer light wavelengths. Incorporating RP into composites enables precise control of the local heat temperature induced by NIR radiation during traditional PTT treatment. This approach minimizes hyperthermia-related damage to non-tumor cells while still effectively targeting tumor cells.[34,35]

We designed a NIR light-responsive Hittorf's phosphorus (HP) modified with PCN (PCN@HP) via a chemical vapor deposition (CVD) strategy in this study. The vertical growth of HP nanorods on PCN revealed a broad and strong optical absorption up to 1000 nm. Under NIR irradiation, this hybrid exhibited a pronounced inhibitory effect on ccRCC cells both in vitro and in vivo, generating local heat and type I/II PDT ROS, while sparing healthy tissues and cells. Importantly, the composite displayed excellent biocompatibility and self-luminescent properties and could be completely metabolized within 48 h in vivo. We demonstrate the potential of PCN@HP as a versatile nano-agent for highly efficient tumor nano-treatment.

2. Results and Discussion

2.1. Characterization of the PCN@HP(x) Hybrid

The heterostructured PCN@HP(x) was synthesized through the CVD approach by calcining the mixture of amorphous RP and PCN at 450 °C (**Figure 1a**). Subsequently, the as-prepared samples were characterized, X-ray diffraction (XRD) analysis determined the phase composition of PCN@HP(x) (Figure 1b). Two distinct diffraction peaks at 13.3° and 27.7°, corresponding to PCN, and additional peaks at 15.4° and 34.2°, attributed to HP, were observed in the PCN@HP(x) samples. Scanning electron microscopy (SEM) and transmission electron microscopy (TEM) were used to assess the morphological and surface characteristics of the prepared samples. The SEM (Figure 1c,d) and TEM images (Figure 1e,f) revealed that the vertically anchored, 1D, rod-like HP structures, with a length of 1–2 μm and a diameter of tens of nanometers, were attached to PCN. Moreover, the[110] facet of well-crystallized HP is assigned to the lattice fringes with a *d*-spacing of 0.275 nm (Figure 1g). The successful deposition of HP on PCN was further confirmed by the uniform distribution of C, N, and P signals in the energy-dispersive X-ray spectroscopy (EDS) elemental mapping images of PCN@HP(0.5) composites (Figure 1h).

The X-ray photoelectron spectroscopy (XPS) survey spectra of the as-prepared samples indicated the elemental chemical states of PCN@HP (Figure S2a, Supporting Information). In the C 1s spectra (**Figure 2a**), two peaks were observed at 288.1 and 284.8 eV, corresponding to sp2-hybridized carbons within an N-containing aromatic ring (N−C═N) and graphitic carbon (C═C−C), respectively. The N 1s spectra (Figure 2b) exhibited three distinct peaks: 401.1 eV (amino functions carrying hydrogen, C−N−H), 399.8 eV (tertiary nitrogen, C−N groups), and 398.6 eV (sp2-hybridized nitrogen in triazine rings, C═N−C). The P 2p XPS spectra for PCN@HP(x) displayed three peaks at 129.7, 130.6, and 133.6, corresponding to elemental phosphorus (2p3/2 and 2p1/2), and P−N bonds formed between RP and CN (Figure 2c), respectively. Consistent with the XRD result, the successful fabrication of PCN@HP(x) heterostructures was further confirmed by Raman spectra (Figure S2b, Supporting Information). Furthermore, the negative zeta potentials of the samples in PBS suspensions suggest a tendency to settle on the cell membrane (Figure 2d).

2.2. The Optical, Photothermal and Photodynamic Properties of the PCN@HP(x) Hybrid

The red-brown color of PCN@HP(x) hybrid aqueous solutions suggests that the obtained PCN@HP(x) heterostructures are favorable to NIR light harvesting (Figure S1, Supporting

L. Zhang
Medizinische Klinik und Poliklinik IV
Ludwig-Maximilians-Universität München
80339 Munich, Germany

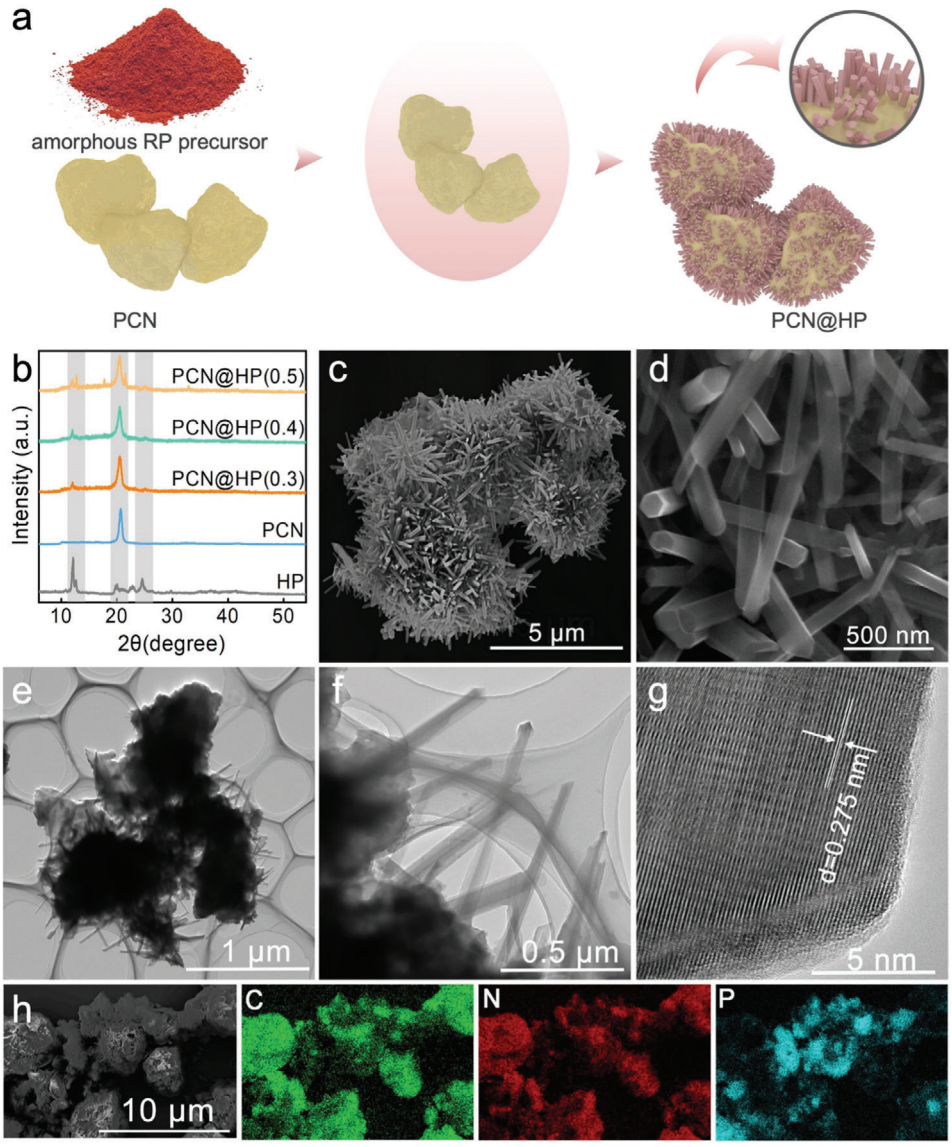

Figure 1. Characterization of PCN@HP heterostructure. a) Schematic diagram of the synthetic process of PCN@HP. b) XRD patterns of HP, PCN, and PCN@HP(x). c,d) SEM images of PCN@HP(0.5). e,g) TEM images of PCN@HP(0.5). h) corresponding EDS mapping images of PCN@HP(0.5).

Information).[36] Then, the high photothermal conversion performance of PCN@HP(x) was further verified. PCN@HP(x) exhibits enhanced light absorption in the visible and NIR regions, making it a potential candidate for NIR-driven PDT and PTT (**Figure** 3a). This indicates the desired NIR absorption and excellent photothermal conversion efficiency, which are essential for photothermal reagents in PTT. Upon 808 nm laser irradiation, the temperature of the solution steadily increases, reaching 70.1 °C after 15 min, indicative of an excellent photothermal effect (Figure 3b). Based on the fact that temperatures exceeding 50 °C can cause damage to normal tissues,[37] different concentrations of PCN@HP(x) were evaluated to determine the optimal therapeutic concentration. As a result, PCN@HP(0.5) exhibited a dose-dependent photothermal conversion efficiency. At a dose of 60 μg mL^{-1}, the temperature increases from 25.0 to 42.1 °C after 10 min of NIR irradiation, a temperature range widely used in cancer treatment (Figure 3c).[38] Furthermore, the photothermal conversion performance of PCN@HP(x) at various concentrations and NIR power densities was investigated, revealing a direct correlation between temperature and power density (Figure 3d). Additionally, there is minimal attenuation of the photothermal effect after three laser cycles, indicating that PCN@HP exhibits exceptional photostability (Figure S3a,b, Supporting Information). Furthermore, electron paramagnetic resonance (EPR) spectra validated that PCN@HP(0.5) can generate $^1O_2$, $\bullet O_2^-$ and •OH under irradiation at 808 nm wavelength (Figure 3e–g). Moreover, the single Lorentzian line centered at g = 2.003 can be observed, which is attributed to the generation of unpaired electrons in PCN@HP(0.5) (Figure 3h).[39]

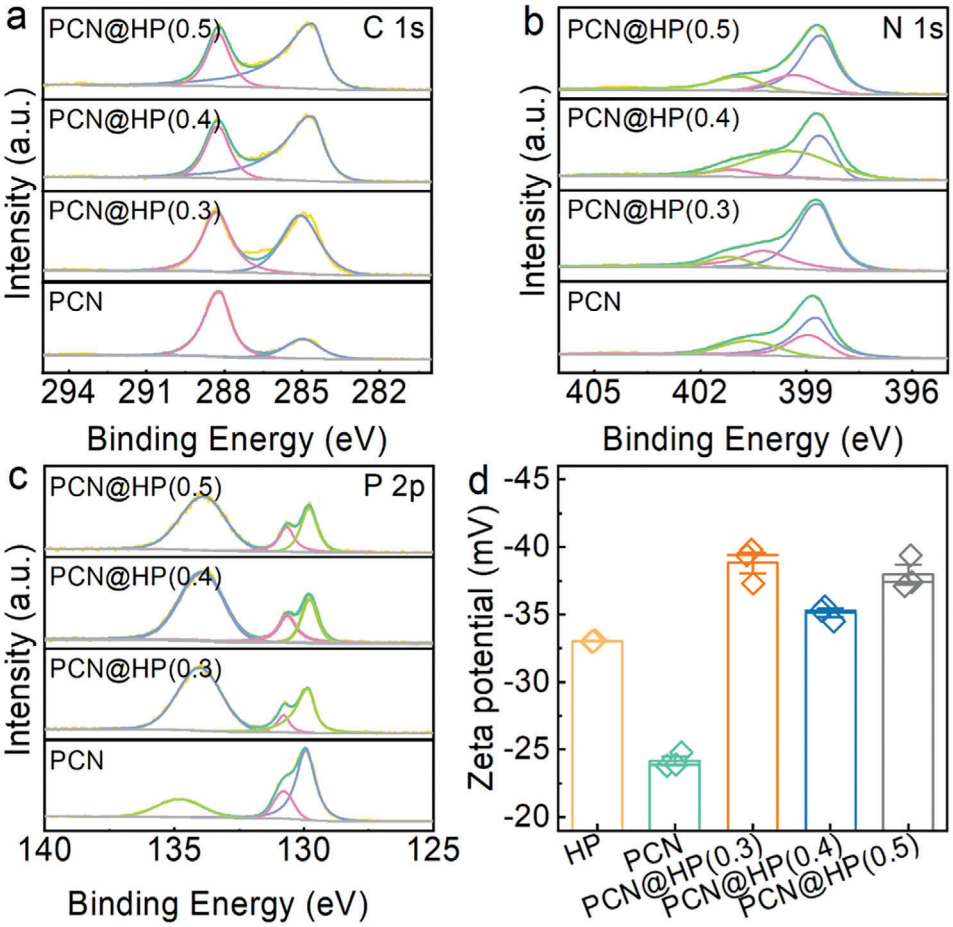

Figure 2. High-resolution XPS spectra of a) C 1s, b) N 1s, and c) P 2p, and d) zeta potentials of HP, PCN, and PCN@HP(x) in PBS.

Collectively, PCN@HP(x) heterostructure exhibits excellent photothermal performance as photothermal agents under NIR irradiation and has the potential for PTT. The underlying mechanism may lie in the broad absorption spectra induced by RP, which produces local heat under NIR irradiation. Furthermore, the PCN@HP heterojunction facilitates charge migration and separation, leading to a significant increase in ROS generation through two pathways: type-I, involving $\bullet O_2^-$, •OH radicals, and H_2O_2, and type-II, involving $^1O_2$.[40–42]

2.3. PDT/PTT Effects Induced by PCN@HP(x) Hybrid In Vitro

The effect of PCN@HP(x) on ccRCC cells (786-O) and human renal tubular epithelial cells (HK-2) was evaluated due to its effective PTT and PDT capabilities under NIR irradiation. Results showed that a 10-min irradiation of 808 nm, which has good penetration depth and no overheating problem,[43] at a power of 2.0 W cm^{-2} without PCN@HP(x) incubation did not cause any cytotoxic effects on HK-2 or ccRCC cells (**Figure 4**), indicating the potential application of NIR-driven PTT and PDT.[44] In contrast, the survival rate of ccRCC cells decreased to less than 50% when exposed to PCN@HP(x) under NIR irradiation at a dose of 60 μg mL^{-1} (Figure 4a; Figure S4a–c, Supporting Information). However, the survival rate of HK-2 cells remained unchanged under the same conditions (Figure 4b; Figure S4d–f, Supporting Information) Remarkably, although DOX treatment, a widely used anti-tumor drug in clinical practice, exhibited robust tumor-killing efficacy, it also led to a significant decrease in HK-2 cell viability at equivalent concentrations compared to PCH@HP (Figure 4c). This highlights the superior safety profile of PCN@HP and its potential for clinical application. Additionally, a significant reduction in tumor cell number and a morphological change from elongated spindle-shaped cells to wrinkled and long forms with damaged cell membranes can be observed, indicating a condition of cell breakdown induced by PCN@HP hybrid (Figure 4d). Moreover, the Hoechst staining assay exhibited chromatin condensation, fragmentation, and the formation of apoptotic bodies in both the PCN@HP and PCN@HP-NIR groups, with the PCN@HP-NIR group demonstrating more pronounced cellular damage (Figure 4e).

EdU staining was conducted to assess the effect of the PCN@HP hybrid on ccRCC cell proliferation. Results indicated that NIR irradiation had negligible impact on the proliferation of ccRCC cells, while the PCN@HP hybrid inhibited it to a certain extent. Notably, a cessation of proliferation in the majority of cells was observed in the PCN@HP-NIR group (Figure S5a–c, Supporting Information). Then, qRT-PCR analysis was

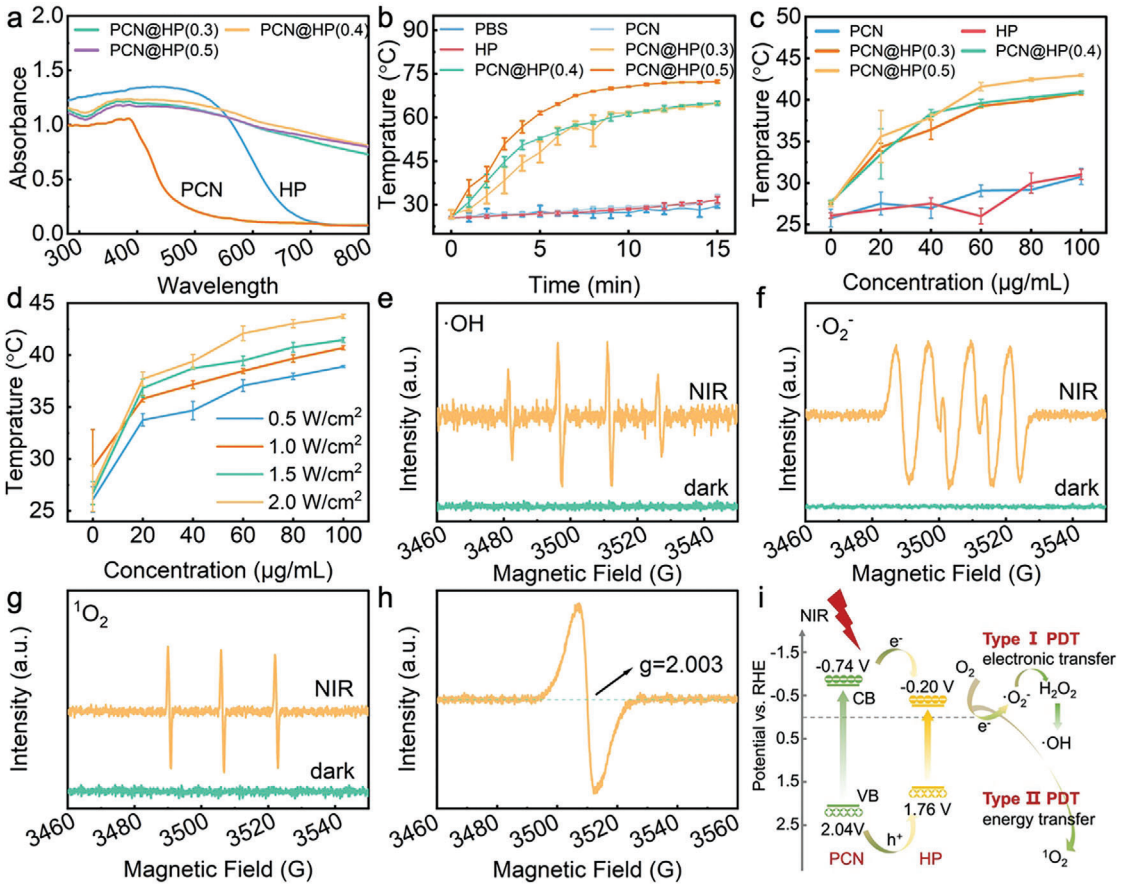

Figure 3. The optical, photothermal, and photodynamic properties of the PCN@HP(x). a) UV-vis-NIR spectra were obtained for PCN@HP(x). b) The temperature variation of PCN@HP(x) at a concentration of 1 mg mL^{-1} monitored during irradiation for varying durations. c) The temperature change of PCN@HP(x) at different concentrations measured under NIR laser irradiation for 10 min. d) The temperature change of PCN@HP(0.5) at various concentrations examined under different power densities of laser. EPR spectra of e) DMPO-•OH adducts, f) DMPO-•O_2^- adducts, and g) TEMP-$^1O_2$ adducts over PCN@HP(0.5) under dark and NIR = 808 nm irradiation conditions. h) EPR spectra of PCN@HP(0.5) under dark condition. i) a schematic illustration of the enhanced ROS generation mechanism by PCN@HP(0.5).

conducted to confirm the cell breakdown induced by the intervention. Figure S7a–c (Supporting Information) shows that the relative expression of typical apoptosis markers, including Caspase-3, Bax, and Bad, were significantly elevated in the PCN@HP-NIR group compared to the other groups.[45] The relative expression of other typical indicators relating to inflammation, oxidative stress, and necrosis also exhibited marked differences between groups treated with and without PCN@HP. Though no significant difference was found between the groups undergoing NIR and non-NIR treatments, the mRNA levels of all injury indicators were higher in the NIR groups (Figure S6d–f, Supporting Information). In conclusion, PCN@HP(x) combined with NIR irradiation represents a dual therapeutic strategy that integrates PTT and NIR irradiation for tumor treatment.

2.4. PDT/PTT Effects Induced by PCN@HP(x) Hybrid In Vitro

In vitro experiments were conducted to further verify the PDT mechanism on PCN@HP under NIR irritation. First, the fluorescence intensity of ROS and its subtypes including $^1O_2$, •OH, •O_2^-, and H_2O_2, were detected using specific fluorescent probes.[46–49] As shown in **Figure 5a–f**, the fluorescence intensity of ROS and its subtypes increased rapidly after 24 h of co-incubation of ccRCC and PCN@HP hybrid, indicating the ability of PCN@HP to kill tumor cells without NIR irradiation. However, the fluorescence amplified when with NIR, providing evidence for the synergistic therapeutic effect of PCN@HP under NIR irradiation. Then, qRT-PCR analysis was employed to validate the generation of ROS within cells. The upregulation of cellular HO-1 levels serves as a hallmark of oxidative stress, particularly under pro-oxidative conditions. Figure 5g illustrates a marked upregulation of HO-1 in PCN@HP-treated groups and the PCN@HP-NIR group. Remarkably, the PCN@HP group exposed to light irradiation exhibited significantly higher levels of HO-1 compared to the non-NIR-treated groups. NRF2, a regulator of ROS in cancer cells,[50,51] showed significant suppression of expression across all concentrations of PCN@HP and PCN@HP NIR groups, with no significant difference between PCN@HP groups with and without NIR treatment (Figure 5h). Interestingly, the relative expression of p53, a regulator of ROS in cancer development and cell death,[52] was notably decreased in both the

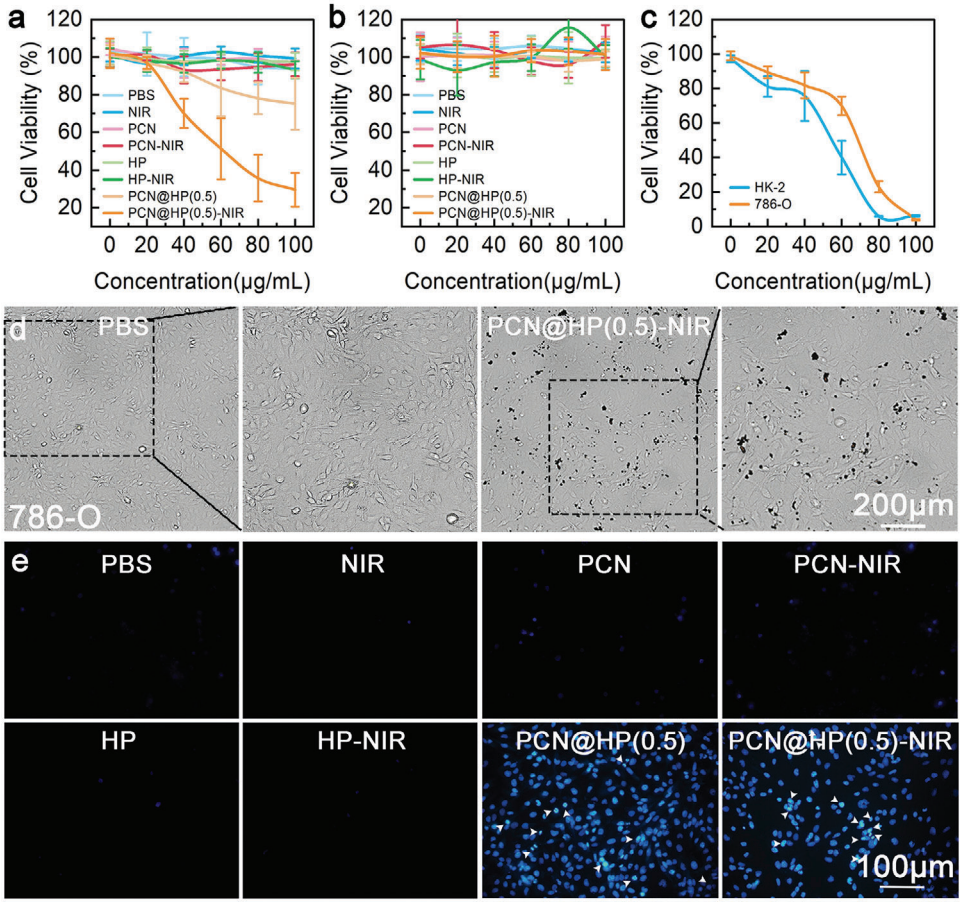

Figure 4. Cytotoxicity of PCN@HP(0.5) was detected using the CCK-8 method in a) 786-O cells, and b) HK-2 cells. c) Cytotoxicity of DOX in 786-O and HK-2 cells. d) The morphologies of 786-O cells of control and PCN@HP(0.5)-NIR treated cultures. e) Hoechst staining of control, mere NIR, PCN@HP(0.5), PCN@HP(0.5)-NIR groups.

PCN@HP and NIR-PCN@HP treated groups. This downregulation may represent a preventive mechanism against excessive oxidative stress (Figure 5i).[53] The results highlight the strong ability of the PCN@HP hybrid to induce ROS. Additionally, the inhibition of ccRCC cell viability in the absence of light suggests that the cell death resulting from co-culturing PCN@HP with ccRCC cells under NIR irradiation is not solely attributable to the photothermal effect.

2.5. The Synchronous Effects of PCN@HP(x) Hybrid In Vivo

To confirm the therapeutic efficacy and the underlying mechanism of PCN@HP hybrid for ccRCC in vivo, a 786-O tumor xenograft Balb/c nude mice model was used in this study (**Figure 6a**).[54] The tumor size showed immediate shrinkage after PCN@HP-NIR administration, indicating the potent tumor growth inhibition efficacy of NIR-mediated PDT/PTT (Figure S7, Supporting Information). Administration of PCN@HP hybrid followed by 10-min NIR irradiation elevated the tumor's local temperature to a peak of 46.7 °C, in contrast to the control group where irradiation alone raised the temperature to 35.7°± 0.6 C and PCN@HP hybrid without NIR irradiation to 35.5° ± 0.4 C. This discovery highlights PCN@HP as a promising photosensitizer for PDT/PTT (Figure 6b; Figure S8, Supporting Information). As depicted in Figure 6c,d, a 7-day treatment period, the tumor volume of mice from both the PBS group and NIR group exhibited continuous growth. Conversely, consistent with the in vitro results, mice treated with PCN@HP(0.5) showed a slight reduction in tumor size; however, upon NIR irradiation, the tumor size of mice in the PCN@HP(0.5) NIR group was halved. The changes observed in tumor weight (Figure 6e) further substantiate the synergistic therapeutic efficacy of PDT and PTT on tumors. Furthermore, histological analysis of tumor tissues was conducted using H&E staining. Tumor tissues from the control and single NIR treatment groups displayed no damage, with the proliferation of spindle-shaped carcinoma cells arranged in fascicular patterns. In contrast, significant damage was observed in the tumor cells of the NIR-mediated PCN@HP groups, where cells were completely lost or reduced compared to the moderately damaged cells in the PCN@HP group (Figure 6f). The TUNEL assay was employed to assess the apoptotic status of various groups. Only several physiologically apoptotic cells were detected in the control group, indicating the suitability of 808 nm NIR as an in vivo illuminant. In the PCN@HP group, a higher number of TUNEL-positive cells were observed, with the greatest

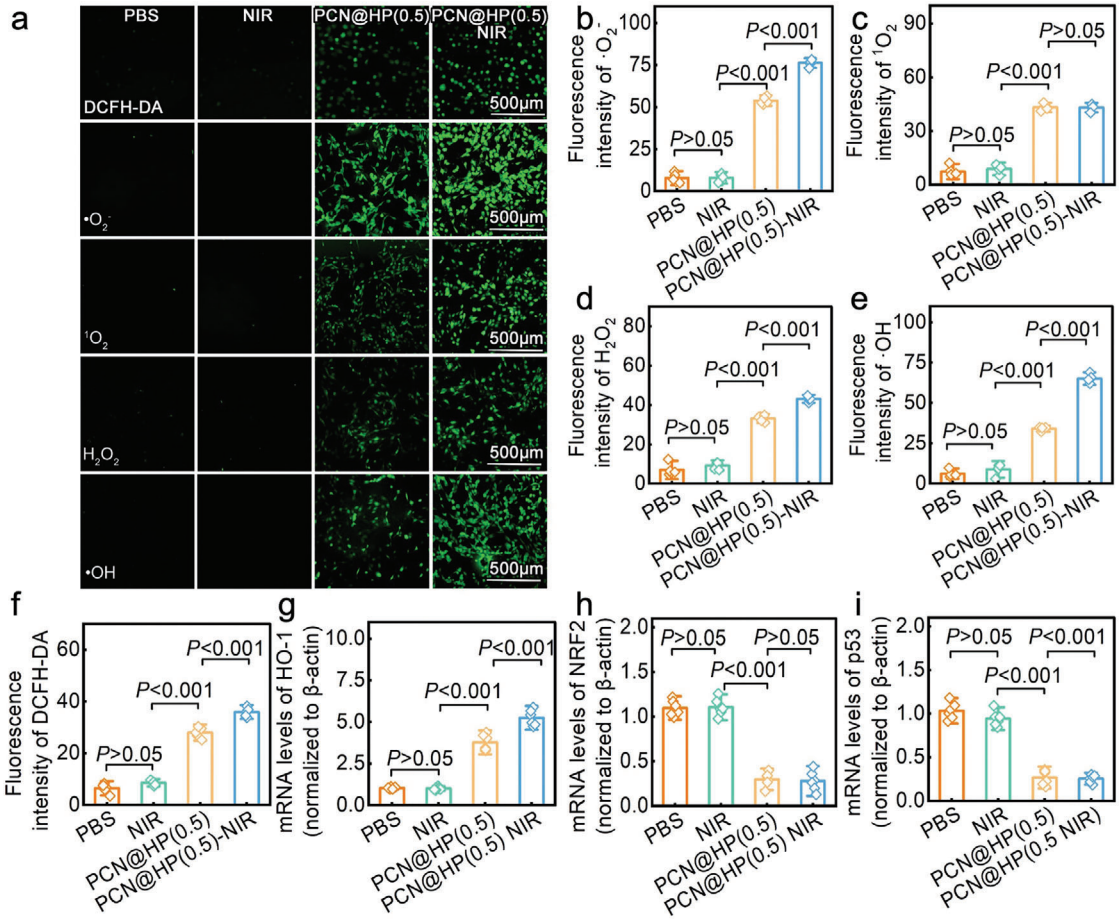

Figure 5. a) Fluorescence intensity and quantification of b) $\bullet O_2^-$, c) $^1O_2$, d) H_2O_2, e) •OH and f) ROS of ccRCC cells in control, NIR, PCN@HP and PCN@HP-NIR treated groups. mRNA levels of g) HO-1 and h) NRF2 and i) p53.

level of apoptotic ccRCC cells observed upon NIR laser exposure (Figure 6g). Caspase-3 expression, a protein related to apoptosis, was evaluated.[55] The PCN@HP-NIR group displayed elevated caspase-3 staining, indicating that NIR-mediated PDT boosted caspase-3 protein expression in comparison to the control tumors (Figure 6h). Ki-67 protein, a commonly used proliferation marker for human tumor cells,[56] exhibited decreased levels upon exposure to PCN@HP and PCN@HP-NIR. Specifically, the PCN@HP-NIR group displayed a more substantial reduction in cell numbers and Ki-67 positive rates compared to the non-NIR treatment group. This result concurred with the in vitro NIR-mediated PDT observations, suggesting that PCN@HP-NIR is capable of hindering the proliferation of ccRCC cells in both in vitro and in vivo settings (Figure 6i).

This study evaluated the biocompatibility of the PCN@HP hybrid. The results demonstrated good biosafety in both short-term and long-term treatment, without any significant effects on the survival rate of mice or the function of organs such as the liver and kidneys (**Figure 7**; Figure S9, Supporting Information). Additionally, it can be completely metabolized within 48 h (Figure S10, Supporting Information). These findings highlight the exceptional biosafety of PCN@HP therapy, emphasizing their potential for clinical application.[57]

3. Conclusion

The PCN@HP heterostructure was created from HP nanorods via the CVD method. The inclusion of HP effectively widened the absorption spectra of the resulting PCN@HP heterostructure, allowing for response to 808 nm NIR irradiation. Upon exposure to NIR irradiation, the PCN@HP heterostructure displayed synchronized therapeutic abilities, effectively producing cytotoxicity ROS and localized heat for the treatment of ccRCC. PCN@HP displayed strong anti-tumor effects in vitro and in vivo, capitalizing on the synergistic potential of PTT and type I/II PDT. This study showcases the PCN@HP hybrid's potential as a promising agent for ccRCC treatment, providing novel insights into therapeutic strategies and emphasizing the clinical potential of synchronizing type I/II PDT and PTT regimens for this context.

4. Experimental Section

Photothermal Properties of PCN@HP(x) Hybrid In Vitro: The UV-vis diffuse reflectance spectra were detected using an Agilent Cary 5000 UV-vis-NIR spectrophotometer equipped with an integrated sphere accessory. Then to evaluate the photothermal performance, solutions of

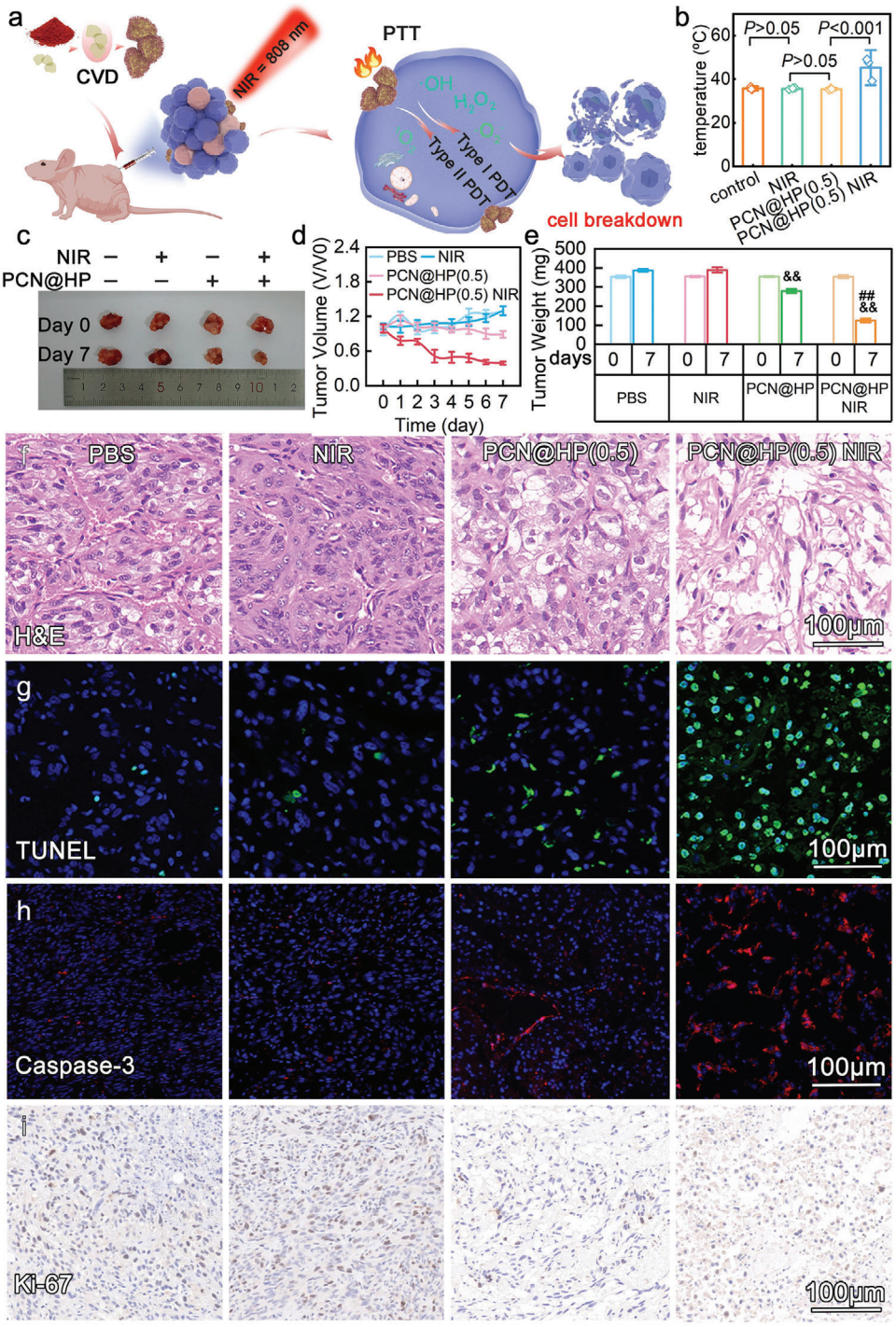

Figure 6. a) The proposed mechanism for photocatalytic tumor-killing effect by PCN@HP(0.5). b) Temperature change of different groups of tumor-bearing mice. c) Photomicrographs depicting tumors collected from the various treatment groups before and after a 7-day treatment period. d) Tumor volume in different groups treated for varying durations (mean ± standard deviation, n = 5). e) Tumor weight in different groups (mean ± standard deviation, n = 5). $^{\&\&}p$ <0.001 versus day 0; $^{\#\#}p$ <0.001 versus PCN@HP at day 7; In vivo f) H&E, g) TUNEL assay, h) Caspase-3 and i) Ki-67 images of control, NIR-treated, PCN@HP(0.5) treated, and PCN@HP(0.5)-NIR treated ccRCC tumors.

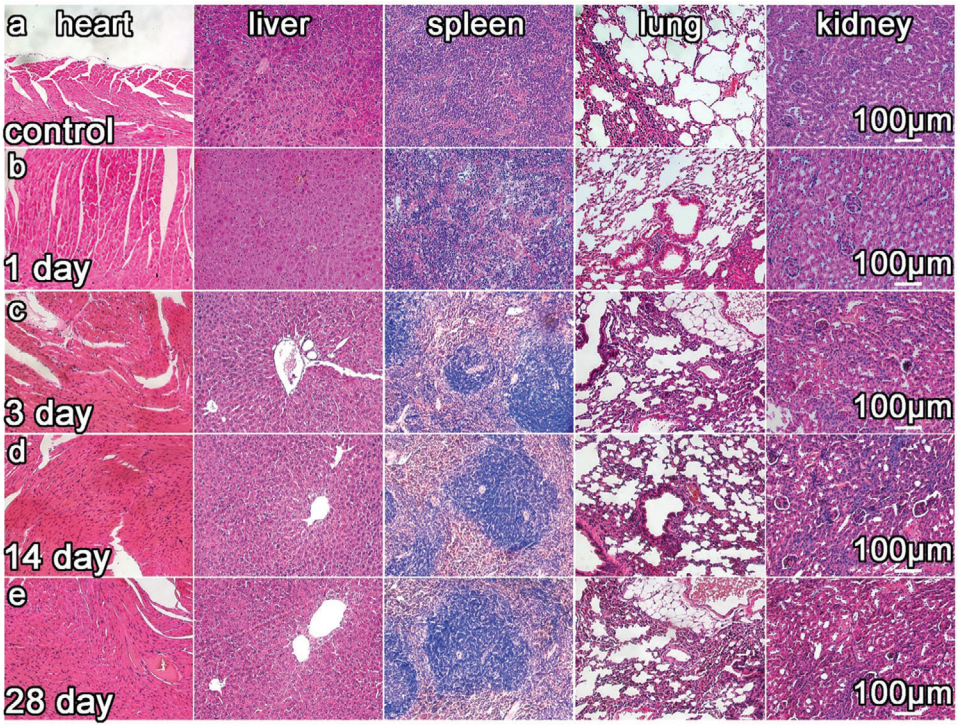

Figure 7. H&E staining images of a) normal organs and b–e) organs after PCN@HP treatment on different days.

PCN@HP(x) with varying concentrations (0, 20, 40, 60, 80, and 100 μg mL^{-1}) were placed in 12-well plates and irradiated with near-infrared light at a wavelength of 808 nm and a power density of 2.0 W cm^{-2} for 10 min. The temperature of the solutions was monitored using an infrared thermographic camera (IRT, Ti400, Fluke, USA). To assess the power controllability of the PCN@HP(x) solution, it was diluted to a concentration of 100 μg mL^{-1} and irradiated with different power densities of 0.5, 1.0, and 2.0 W cm^{-2} for 10 min. The temperature changes of the PCN@HP(x) solution at various concentrations and power densities were recorded at 60-s intervals. To evaluate the photothermal stability of the system, a suspension of PCN@HP hybrid at a concentration of 100 μg mL^{-1} was subjected to repeated ON/OFF cycles of irradiation using an 808 nm NIR laser with a power density of 2.0 W cm^{-2}. The photothermal conversion efficiency was determined by irradiating 1 mL of the PCN@HP hybrid aqueous dispersion (100 μg mL^{-1}) continuously under the same conditions until a steady-state temperature was achieved. The temperature decrease was recorded after turning off the laser.

In Vivo Treatment: Male nude mice (4-5 weeks old, 18–20 g) were obtained from Vital River Laboratory Animal Technology Co., Ltd (Beijing, China) and individually housed in isolated cages with independent air supply. The mice were kept at a room temperature of 21 ± 2 °C and a relative humidity of 50% ± 15%. Food and water were available ad libitum. Initially, 1×10^6 786-O cells suspended in RPMI 1640 medium and mixed with Matrigel (Corning, NY, USA) at a 1:1 ratio were injected into the axillary subcutaneous tissue of male nude mice. When the tumor volume reached 100 mm^3, the mice were randomly assigned to four groups ($N = 5$ per group): PBS, NIR, PCN@HP hybrid, and PCN@HP-NIR. The intratumoral injection was performed using 1 mg mL^{-1} (100 μL) solutions. After four h, the tumor sites were exposed to an 808 nm laser (2.0 W cm^{-2}, 10 min), and temperature images were captured using a TiS20 thermal imaging system (FLUKE, Everett, WA, USA). The tumors from the treated mice were collected 24 h after various treatments for H&E, TUNEL, Ki-67, and Caspase-3 staining to investigate the therapeutic effect.

Supporting Information

Supporting Information is available from the Wiley Online Library or from the author.

Acknowledgements

This work was supported by the National Natural Science Foundation of China (Nos. 81970582, 82270724, 52102362), Qingdao Key Health Discipline Development Fund, Qingdao Key Clinical Specialty Elite Discipline, Taishan Scholar Program of Shandong Province (No. tstp 20230665), and Shandong Provincial Natural Science Foundation (ZR2021QB022). No funding bodies had any role in study design, data collection and analysis, publication decisions, or manuscript preparation. The authors thank all those colleagues who provided support and help in various ways to this study. [Author contributions and the funding sources in the Acknowledgements have been added on 28 March 2024, after original online publication.]

[Correction added on March 28, 2024: The author contribution section is added and acknowledgement section has been corrected in this version]

Conflict of Interest

The authors declare no conflict of interest.

Author Contributions

Y. Xu, Y.K. Zhu and D.H. Li designed and guided the overall research project. C. Guan designed the experiments, wrote the manuscript and performed the data analysis. C.Y. Li, C.Y. Yang, D.J. Yang, L.X. Zhang provided intellectual input, helped interpret the results and polished the

manuscript. L.Y. Xu and K. Liu were involved in the material synthesis and characterization. N.X. Zhang, T.Y. Li and Z. Song assisted in in vivo experiments. L. Che and Y.F. Wang were involved in in vitro experiments. L.W. Zhang helped polish the manuscript. All authors were involved in the writing of the manuscript and the decision to submit the manuscript for publication. The manuscript was written through the contributions of all authors. All authors have given approval to the final version of the manuscript.

Data Availability Statement

The data that support the findings of this study are available from the corresponding author upon reasonable request.

Keywords

clear cell renal cell carcinoma, Hittorf's phosphorus, mild photothermal therapy, photodynamic therapy

Received: December 27, 2023
Revised: February 18, 2024
Published online:

[1] A. Siddiqi, M. Rani, P. Bansal, M. M. A. Rizvi, *Life Sci.* **2022**, *308*, 120922.
[2] B. Cheng, M. Xie, Y. Zhou, T. Li, W. Liu, W. Yu, M. Jia, S. Yu, L. Chen, R. Dai, R. Wang, *Cell Death Discov.* **2023**, *9*, 121.
[3] B. I. Rini, M. B. Atkins, *Lancet Oncol.* **2009**, *10*, 992.
[4] C. Krishna, R. G. DiNatale, F. Kuo, R. M. Srivastava, L. Vuong, D. Chowell, S. Gupta, C. Vanderbilt, T. A. Purohit, M. Liu, E. Kansler, B. G. Nixon, Y. B. Chen, V. Makarov, K. A. Blum, K. Attalla, S. Weng, M. L. Salmans, M. Golkaram, L. Liu, S. Zhang, R. Vijayaraghavan, T. Pawlowski, V. Reuter, M. I. Carlo, M. H. Voss, J. Coleman, P. Russo, R. J. Motzer, M. O. Li, et al., *Cancer Cell* **2021**, *39*, 662.
[5] J. C. Penticuff, N. Kyprianou, *Am. J. Clin. Exp. Urol.* **2015**, *3*, 77.
[6] S. Siva, G. Kothari, A. Muacevic, A. V. Louie, B. J. Slotman, B. S. Teh, S. S. Lo, *Nat. Rev, Urol.* **2017**, *14*, 549.
[7] Y. Li, T. M. Lih, S. M. Dhanasekaran, R. Mannan, L. Chen, M. Cieslik, Y. Wu, R. J. Lu, D. J. Clark, I. Kołodziejczak, R. Hong, S. Chen, Y. Zhao, S. Chugh, W. Caravan, N. Naser Al Deen, N. Hosseini, C. J. Newton, K. Krug, Y. Xu, K. C. Cho, Y. Hu, Y. Zhang, C. Kumar-Sinha, W. Ma, A. Calinawan, M. A. Wyczalkowski, M. C. Wendl, Y. Wang, S. Guo, et al., *Cancer Cell* **2023**, *41*, 139.
[8] J. Wang, X. Wu, P. Shen, J. Wang, Y. Shen, Y. Shen, T. J. Webster, J. Deng, *Int. J. Nanomed.* **2020**, *15*, 1903.
[9] C. Zhao, X. Han, S. Wang, Z. Pan, X. Tang, Z. Jiang, *Adv. Healthcare Mater.* **2023**, *12*, 2201995.
[10] K. Liu, Z. Jiang, R. A. Lalancette, X. Tang, F. Jäkle, *J. Am. Chem. Soc.* **2022**, *144*, 18908.
[11] J.-S. Lan, L. Liu, R.-F. Zeng, Y.-H. Qin, J.-W. Hou, S.-S. Xie, S. Yue, J. Yang, R. J. Y. Ho, Y. Ding, T. Zhang, *Chem. Eng. J.* **2021**, *407*, 127212.
[12] C. Xu, Y. Zhou, Z. Li, Y. Zhou, X. Liu, X. Peng, *J. Hazard. Mater.* **2021**, *418*, 126243.
[13] Y. Lin, Q. Yin, D. Tian, X. Yang, S. Liu, X. Sun, Q. Chen, B. Fang, H. Liang, L. Li, D. Zhuge, H. Wang, C. Weng, J. Xu, C. Hu, J. Xie, X. Zhang, L. Yan, X. Lu, F. Wang, C. Liu, Y. Hu, M. Chen, L. Wang, Y. Chen, *ACS Nano* **2023**, *17*, 12160.
[14] C. Yang, Y. Zhu, D. Li, Y. Liu, C. Guan, X. Man, S. Zhang, L. Zhang, D. Yang, Y. Xu, *Small* **2021**, *17*, 2101837.
[15] X. Li, L. Chen, M. Huang, S. Zeng, J. Zheng, S. Peng, Y. Wang, H. Cheng, S. Li, *Asian J Pharm. Sci.* **2023**, *18*, 100775.
[16] X. Yi, Q. Y. Duan, F. G. Wu, *Research* **2021**, *2021*, 9816594.
[17] M. Overchuk, R. A. Weersink, B. C. Wilson, G. Zheng, *ACS Nano* **2023**, *17*, 7979.
[18] H. S. Leong, K. S. Butler, C. J. Brinker, M. Azzawi, S. Conlan, C. Dufés, A. Owen, S. Rannard, C. Scott, C. Chen, M. A. Dobrovolskaia, S. V. Kozlov, A. Prina-Mello, R. Schmid, P. Wick, F. Caputo, P. Boisseau, R. M. Crist, S. E. McNeil, B. Fadeel, L. Tran, S. F. Hansen, N. B. Hartmann, L. P. W. Clausen, L. M. Skjolding, A. Baun, M. Ågerstrand, Z. Gu, D. A. Lamprou, C. Hoskins, et al., *Nat. Nanotechnol.* **2019**, *14*, 629.
[19] M. He, Z. Cheng, Z. Wang, M. Li, H. Liang, H. Liu, L. Yu, L. Zhao, F. Yu, *Adv. Healthcare Mater.* **2023**, *12*, 2300752.
[20] A. Naskar, K. S. Kim, *Pharmaceutics* **2022**, *14*, 2343.
[21] B. Liu, C. Li, G. Chen, B. Liu, X. Deng, Y. Wei, J. Xia, B. Xing, P. Ma, J. Lin, *Adv. Sci.* **2017**, *4*, 1600540.
[22] C. Pan, Z. Mao, X. Yuan, H. Zhang, L. Mei, X. Ji, H. Nanomedicine, *Adv. Sci.* **2022**, *9*, 2105747.
[23] J. Dang, H. He, D. Chen, L. Yin, *Biomater. Sci.* **2017**, *5*, 1500.
[24] S. Liang, Z. Wang, Z. Zhou, G. Liang, Y. Zhang, *Biosens. Bioelectron.* **2022**, *211*, 114370.
[25] C. Zhao, J. Kang, Y. Li, Y. Wang, X. Tang, Z. Jiang, *Cyborg. Bionic Syst.* **2023**, *4*, 0022.
[26] G. N. Bosio, D. O. Mártire, *Photodiagn. Photodyn. Ther.* **2022**, *37*, 102683.
[27] M. H. Chan, Y. T. Pan, I. J. Lee, C. W. Chen, Y. C. Chan, M. Hsiao, F. Wang, L. Sun, X. Chen, R. S. Liu, *Small* **2017**, *13*, 1700038.
[28] D. W. Zheng, B. Li, C. X. Li, J. X. Fan, Q. Lei, C. Li, Z. Xu, X. Z. Zhang, *ACS Nano* **2016**, *10*, 8715.
[29] H. Zhang, Z. Liu, X. Kang, J. Guo, W. Ma, S. Cheng, *Nanoscale* **2016**, *8*, 2242.
[30] Y. Zhang, T. Mori, J. Ye, M. Antonietti, *J. Am. Chem. Soc.* **2010**, *132*, 6294.
[31] X. Wang, C. An, S. Zhang, S. Wang, J. Li, Y. Zhu, *Sep. Purif. Technol.* **2024**, *340*, 126733.
[32] G. Huang, W. Ye, C. Lv, D. S. Butenko, C. Yang, G. Zhang, P. Lu, Y. Xu, S. Zhang, H. Wang, Y. Zhu, D. Yang, *J. Mater. Sci. Technol.* **2022**, *108*, 18.
[33] Y. Zhu, J. Ren, G. Huang, C.-L. Dong, Y.-C. Huang, P. Lu, H. Tang, Y. Liu, S. Shen, D. Yang, *Adv. Funct. Mater.* **2023**, *34*, 2311623.
[34] X. He, S. Zhang, Y. Tian, W. Cheng, H. Jing, *Int. J. Nanomed.* **2023**, *18*, 1433.
[35] K. Liu, L. Zhang, H. Lu, Y. Wen, B. Bi, G. Wang, Y. Jiang, L. Zeng, J. Zhao, *J. Nanobiotechnol.* **2023**, *21*, 64.
[36] S. L. Higgins, K. J. Brewer, *Angew. Chem. Int. Ed. Engl.* **2012**, *51*, 11420.
[37] C. Wang, L. Xu, C. Liang, J. Xiang, R. Peng, Z. Liu, *Adv. Mater.* **2014**, *26*, 8154.
[38] H. C. Huang, K. Rege, J. J. Heys, *ACS Nano* **2010**, *4*, 2892.
[39] C. Zhou, Z. Zeng, G. Zeng, D. Huang, R. Xiao, M. Cheng, C. Zhang, W. Xiong, C. Lai, Y. Yang, W. Wang, H. Yi, B. Li, *J. Hazard. Mater.* **2019**, *380*, 120815.
[40] Y. Zhu, C. Lv, Z. Yin, J. Ren, X. Yang, C.-L. Dong, H. Liu, R. Cai, Y.-C. Huang, W. Theis, S. Shen, D. Yang, *Angew. Chem., Int. Ed.* **2020**, *59*, 868.
[41] C. Yang, Y. Zhu, D. Li, Y. Liu, C. Guan, X. Man, S. Zhang, L. Zhang, D. Yang, Y. Xu, *Small* **2021**, *17*, 2101837.
[42] J. Chen, Y. Zhu, X. Yang, W. Ye, J. Liu, D. S. Butenko, P. Lu, P. Meng, Y. Xu, D. Yang, S. Zhang, *ACS Appl. Nano Mater.* **2022**, *5*, 862.
[43] X. Zhang, Z. Guo, J. Liu, G. Tian, K. Chen, S. Yu, Z. Gu, *Sci. Bull.* **2017**, *62*, 985.
[44] A. Yuan, J. Wu, X. Tang, L. Zhao, F. Xu, Y. Hu, *J. Pharm. Sci.* **2013**, *102*, 6.
[45] M. Y. Sim, M. L. Go, J. S. P. Yuen, *Life Sci.* **2018**, *203*, 282.
[46] Y. Chen, W. Ai, X. Guo, Y. Li, Y. Ma, L. Chen, H. Zhang, T. Wang, X. Zhang, Z. Wang, *Small* **2019**, *15*, 1902352.

[47] R. L. Siegel, K. D. Miller, A. Jemal, *CA Cancer J. Clin.* **2020**, *70*, 7.
[48] O. Vafa, M. Wade, S. Kern, M. Beeche, T. K. Pandita, G. M. Hampton, G. M. Wahl, *Mol. Cell* **2002**, *9*, 1031.
[49] Y. Shang, Q. Wang, J. Li, H. Liu, Q. Zhao, X. Huang, H. Dong, W. Chen, R. Gui, X. Nie, *Front. Chem.* **2021**, *9*, 522708.
[50] K. Bensaad, A. Tsuruta, M. A. Selak, M. N. Vidal, K. Nakano, R. Bartrons, E. Gottlieb, K. H. Vousden, *Cell* **2006**, *126*, 107.
[51] S. K. Chiang, S. E. Chen, L. C. Chang, *Cells* **2021**, *10*, 2401.
[52] M. Rojo de la Vega, E. Chapman, D. D. Zhang, *Cancer Cell* **2018**, *34*, 21.
[53] T. J. Humpton, A. K. Hock, O. D. K. Maddocks, K. H. Vousden, *Cancer Metab.* **2018**, *6*, 18.
[54] Y. Liu, H. Lv, X. Li, J. Liu, S. Chen, Y. Chen, Y. Jin, R. An, S. Yu, Z. Wang, *Int. J. Biol. Sci.* **2021**, *17*, 3522.
[55] X. Yu, G. Xing, S. Sheng, L. Jin, Y. Zhang, D. Zhu, L. Mei, X. Dong, F. Lv, *Adv. Sci.* **2023**, *10*, 2207456.
[56] X. Sun, P. D. Kaufman, *Chromosoma* **2018**, *127*, 175.
[57] E56 Committee, *Standard Test Method for Analysis of Hemolytic Properties of Nanoparticles*, ASTM International, https://www.astm.org/e2524-22.html, **2022.**